JOURNAL OF CHEMICAL ENGINEERING AND INDUSTRIAL BIOTECHNOLOGY (JCEIB)
ISSN: 2600-7347 e-ISSN: 0126-8139
VOL. 08, ISSUE 02, 1 – 8
DOI: https://doi.org/10.15282/jceib.v8i2.8716

ORIGINAL ARTICLE

Adsorption of Pb(II) from Aqueous Solution Using Dendritic Fibrous Type SBA-15 (DFSBA-15)

R.S.R. Mohd Zaki[1], H.D. Setiabudi[1,2,*], N.H.N. Kamarudin[3], B.A. Abdulkadir[4]

[1]Faculty of Chemical and Process Engineering Technology, Universiti Malaysia Pahang, Lebuhraya Persiaran Tun Khalil Yaakob, 26300 Kuantan, Pahang, Malaysia.
[2]Centre for Research in Advanced Fluid & Processes, Universiti Malaysia Pahang, Lebuhraya Persiaran Tun Khalil Yaakob, 26300 Kuantan, Pahang, Malaysia.
[3]Department of Chemical and Process Engineering, Faculty of Engineering and Built Environment, Universiti Kebangsaan Malaysia, Bangi, Malaysia.
[4]Department of Chemistry, Faculty of Science, Gombe State University, P. M. B. 127, Gombe, Gombe State, Nigeria.

ABSTRACT – The presence of heavy metals in the environment is undeniably harmful and toxic to living things, where the presence of Pb(II) inside human foods and drinks results in various diseases. The use of adsorption as a method of wastewater treatment is widespread, and effective adsorption performance depends on appropriate adsorbent selection. In this research, dendritic fibrous type SBA-15 (DFSBA-15) was prepared and used for lead (Pb(II)) adsorption. The physicochemical properties of the DFSBA-15 were characterized using TEM, BET, and FTIR. The characterization analyses confirmed the formation of fibrous morphology, moderate surface area, and bulk -OH. Several factors, including contact time (min), adsorbent dosage (g/L), pH, and initial concentration (mg/L), were examined for Pb(II) adsorption. The best adsorption performance (89.88%) was attained at 180 min, 1 g/L of adsorbent dosage, pH 5, and 100 mg/L of Pb(II) initial concentration. Pseudo-second-order reaction type and Langmuir isotherm provided good fits to the experimental data, with $R^2 \geq 0.9943$ and $R^2 = 0.9982$, respectively. In short, the DFSBA-15 exhibits great potential for excellent Pb(II) removal.

ARTICLE HISTORY
Received: 10 Sep. 2022
Revised: 22 Sep. 2022
Accepted: 26 Sep. 2022

KEYWORDS
Adsorption
Dendritic fibrous type
DFSBA-15
Pb(II)

INTRODUCTION

Hazardous substances and heavy metals frequently contaminate water bodies that serve as a source of drinking water during rainy runoff. Heavy metals in aquatic environments have fatal long-term effects, non-biodegradability, and toxic effects [1,2]. The maximum acceptable lead (Pb(II)) concentration in drinking water is less than 0.015 mg/L, and a high concentration of Pb(II) could result in a variety of adverse health effects [3]. Therefore, removing Pb(II) from wastewater is crucial, pushing scientists to continue developing novel strategies for its removal.

Several treatment techniques, including adsorption [4], photocatalytic degradation [5], precipitation [6], and ultrafiltration by the membrane [7], were reported. Among others, adsorption has attracted considerable attention and is widely used to treat industrial wastes, effluents, and water supplies owing to its efficiency and practicability [8]. Additionally, the adsorption method has advantages in terms of its adaptability, does not produce any toxic by-products, low energy requirement, and is inexpensive [9]. However, an appropriate selection of adsorbents is vital for excellent adsorption performance.

Fibrous nano-silica (KCC-1) was firstly discovered in 2010 and has attracted considerable attention in numerous applications attributable to its attractive properties, such as wide pore diameter and high surface area. Unlike the typical pore-based silica materials, KCC-1 is surrounded by a vast amount of dendrimer, thus forming fibrous morphology on it. The unique morphology of KCC-1 renders abundant accessible active sites, which subsequently enhance its performance in several applications. The remarkable properties of KCC-1 induced the attempt to modify conventional silica materials into fibrous-type.

Inspired by the excellent properties of KCC-1, fibrous ZSM-5 (FZSM-5) [10] and dendritic fibrous SBA-15 (DFSBA-15) [10,11] were discovered in recent years. Interestingly, DFSBA-15 consists of a mesopores structure suitable for targeted large molecules, like wastewater. Compared to traditional SBA-15, DFSBA-15 has fibrous morphology, noticeable and accessible adsorption sites, better thermal stability, and considerable dendrimer-derived porosity [13]. Owing to the exciting properties of DFSBA-15, in the present study, DFSBA-15 is used to remove Pb(II) from an aqueous solution. Furthermore, the effect of several parameters, including contact time (min), adsorbent amount (g/L), initial pH, and initial Pb(II) concentration (mg/L), were studied to achieve high removal efficiency.

*CORRESPONDING AUTHOR | H.D. Setiabudi | herma@ump.edu.my

METHOD

Preparation of DFSBA-15

Microwave-assisted microemulsion method was utilized to synthesize DFSBA-15, as described by Chong et al. [12]. Firstly, under constant stirring, SBA-15 was added to the solution containing toluene (98%, Sigma-Aldrich) and butanol (99%, Merck). After 1 hour, TEOS was dropped wisely. At the same time, urea (99.99%, Merck), cetyltrimethylammonium bromide (CTAB) (99.99%, Sigma-Aldrich), and water were mixed and stirred in another beaker. Both solutions were combined after each solution achieved homogeneity, followed by aging in the Teflon-sealed microwave reactor (100 ℃, 12 hours). The slurry was centrifuged at 5,000 rpm, followed by drying (120 ℃, overnight) and calcination (120 ℃, 6 hours).

Adsorbent Characterization

DFSBA-15's morphology was examined using transmission electron microscopy (TEM) (Zeiss Libra 120). DFSBA-15's textural properties were characterized using Brunauer-Emmett-Teller (BET) (Micromeritics ASAP 2010) under N_2 flow. Pre-treatment (300 ℃, 1 hour) was conducted prior to analysis. DFSBA-15's functional group was examined using Fourier Transform Infrared (FTIR) (Spectrometer Nicolet iS5).

Adsorption Procedure

The adsorption procedure was conducted following the method described in the literature [4,14]. The stock solution was produced by adding lead nitrate (99%, Sigma-Aldrich) to distilled water at different concentrations (50 mg/L – 400 mg/L). The Pb(II) solution was continuously stirred while adding DFSBA-15 powder. Hydrochloric acid (HCl, Merck) was used to alter the pH of the solution to acidic, while sodium hydroxide (NaOH, Merck) was employed to modify the solution to alkaline. The samples were collected, followed by centrifugation (8 min, 12,000 rpm) and UV-VIS analysis with the addition of a dithizone reagent. The Pb(II) adsorption was calculated using the following Equations.

$$\text{Removal (\%)} = \frac{C_0 - C_t}{C_0} \times 100 \tag{1}$$

$$Q_t = \frac{C_0 - C_t}{m} \times V \tag{2}$$

C_0 and C_t (mg/L) represent the concentration at initial and at any time, respectively. The amount of an adsorbed Pb(II) at any given time was measured by Q_t (mg/g). The weight of the adsorbent was represented by m (g), and the Pb(II) solution's volume was indicated by V (L).

RESULTS & DISCUSSIONS

Adsorbent Characterizations

Figure 1(A) depicts the FTIR spectra of DFSBA-15. The peaks at 798 cm^{-1} and 1047 cm^{-1} indicated the Si−O−Si band's symmetrical and asymmetrical stretching, respectively [15], while the peak at 437 cm^{-1} was assigned to the vibration of bending Si−O [16]. The band at 3351 cm^{-1} was credited to the bulk −OH stretching vibration on the Si−OH bond. During the hydrothermal preparation of DFSBA-15, water was utilized as a solvent and assisted in forming −OH on the surface [17]. The properties of the synthesized DFSBA-15 are comparable with the findings described by Chong et al. [11].

Figure 1(B) shows the TEM image of DFSBA-15. As illustrated, DFSBA-15 consists of dendritic dendrimer fibres, similar to KCC-1's fibrous nano-silica [18]. This dendrimer's structure, with its open hierarchical fibrous channel, will benefit the reactant mass transfer and increase active site accessibility [18]. The BET analysis discovered that the surface area (SA), pore volume (V_p), and pore diameter (D_p) of the DFSBA-15 are 156 m^2/g, 0.31 cm^3/g, and 7.95 nm, respectively. The moderate SA, large V_p, and broad D_p of DFSBA-15 will be advantageous in the adsorption of Pb(II).

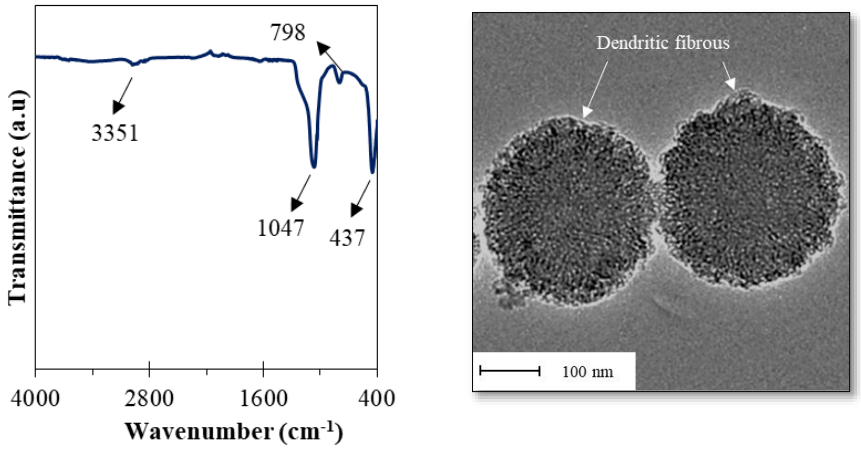

(A) (B)

Figure 1. (A) FTIR spectrum and (B) TEM image of DFSBA-15.

Effects of Parameters for Pb(II) Adsorption

Figure 2 depicts Pb(II) adsorption employing a DFSBA-15 as an adsorbent. Pb(II) adsorption efficiency was 38 % after 60 minutes and progressively raised to 47 % after 180 min. Beyond 180 minutes, the system reached an equilibrium where the adsorption rate remained constant, and a steady-state assumption was predicted. The obtained result is comparable to the study described by Teong et al., wherein the Pb(II) removal rapidly escalated and then gradually raised and remained constant until it reached an equilibrium point [4]. The significant increase in Pb(II) adsorption is owing to the abundant active sites on the DFSBA-15. However, the sluggish adsorption rate above 180 minutes might be due to the less active site availability, and the saturation was reached. Furthermore, the fibrous morphology structure of DFSBA-15 was found to provide a highly accessible active site and allow more Pb(II) pollutants attached to the pores of DFSBA-15, as revealed by the high percentage of Pb(II) removal. This good performance could be ascribed to the moderate SA, large V_p, and broad D_p of the prepared DFSBA-15, as confirmed by BET analysis.

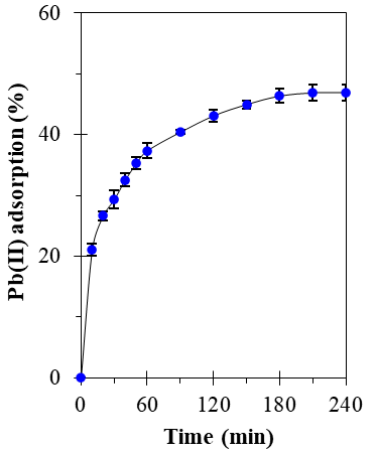

Figure 2. Effect of time on Pb(II) adsorption using DFSBA-15. Condition: C_o = 100 mg/L, pH = 6, m = 0.1 g/L, and T = 30 °C.

Figure 3 depicts the influence of DFSBA-15 dosage on Pb(II) removal. As anticipated, attributable to the abundance of active sites, the Pb(II) removal rate increased as the number of adsorbents DFSBA-15 increased. The Pb(II) adsorption was 48% when the DFSBA-15 dosage was 0.1 g/L but increased to 67% with 1 g/L of DFSBA-15. This is owing to the considerable amount of available binding sites and large surface area, resulting in an increasing number of OH radicals that performed strong interaction with the contaminants molecules (Pb(II)) [19]. On the other hand, as the DFSBA-15 dosage increased from 1 g/L to 5 g/L, the adsorption rate slightly decreased from 67% to 65%. This could be due to the excessive adsorbent of DFSBA-15, where the remaining Pb(II) molecules were unavailable for the adsorption interactions. Hence, 1 g/L of DFSBA-15 is considered the best adsorbent dosage. A similar result was obtained by Song et al., in which Pb(II) adsorption efficiency became higher as the adsorbent dose was added, but no apparent alterations in adsorption percentage after reaching saturation point [20]. In brief, the amount of DFSBA-15 adsorbent loading is directly proportional to the overall adsorption reaction rate as the amount of adsorption is below the saturation stage.

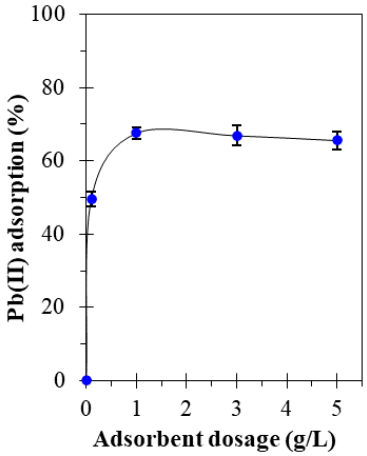

Figure 3. Effect of adsorbent dosage on Pb(II) adsorption using DFSBA-15. Condition: C_o = 100 mg/L, pH = 6, t =180 min, and T = 30 °C.

Figure 4 demonstrates the effect of multiple pHs for Pb(II) adsorption from an aqueous phase. It is evident that modifying the pH from 3 to 5 increases the removal effectiveness from 52% to 77.65%, respectively. This is because the amount of Pb(II) molecule was in cationic forms, and no complexation could occur with less HCl addition [21]. Thus, allowing more Pb(II) to bind to the adsorbent sites. However, the adsorption rate drops progressively in the alkali phase, from 68.24% to 64.14% for pH 8 and 10, respectively. This is owing to OH radicals competing with Pb(II) on the DFSBA-15 surface, slowing down the Pb(II) breakdown and forming $Pb(OH)_2$ precipitate. As observed, pH 5 is considered the best pH for Pb(II) adsorption using DFSBA-15, with Pb(II) removal of 77.65%. The influence of pH followed a similar pattern described by Zhao et al. [22] for Pb(II) adsorption using amorphous Zr-MOG-12 and CzBPOF.

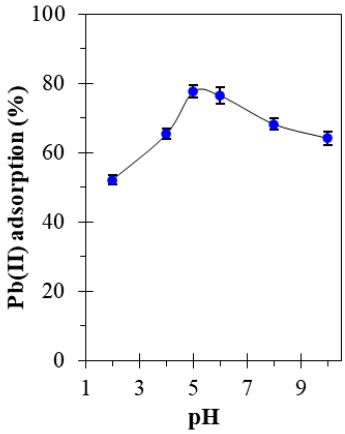

Figure 4. Effect of pH on Pb(II) adsorption using DFSBA-15. Condition: C_o = 100 mg/L, m = 1 g/L, t = 180 min, and T = 30 °C.

Figure 5 presents the effect of various initial Pb(II) concentrations on the Pb(II) adsorption. The figure depicts that increasing initial concentration reduced the efficiency of Pb(II) removal. As indicated, 100 mg/L illustrated the higher Pb(II) removal, followed by 200 mg/L. Nevertheless, a further increase in the initial concentration to 400 mg/L lowered the Pb(II) adsorption percentage, which is 78.11%. This could be due to the less Pb(II) pollutant at a lower concentration (100 mg/L) compared to a higher concentration (400 mg/L), and surface-active sites have become saturated with the pollutant [4]. For the above adsorption study using one-factor-at-one-time (OFAT), the best adsorption performance (89.88%) was attained at 180 min, 1 g/L of adsorbent dosage, pH 5, and 100 mg/L of Pb(II) initial concentration.

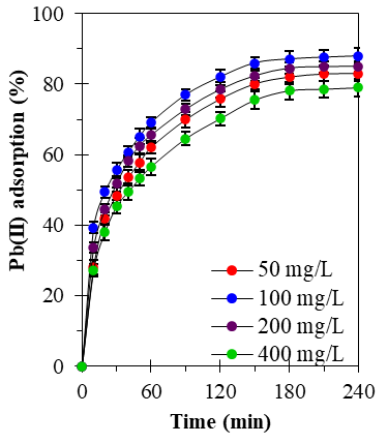

Figure 5. Effect of initial concentration on Pb(II) adsorption using DFSBA-15. Condition: m = 1 g/L, pH = 5, t = 180 min, and T = 30 °C.

Kinetic Study

Pseudo-first-order (PFO), pseudo-second-order (PSO), and Elovich kinetic models were deployed under the effect of initial concentrations (C_o = 50 mg/L - 400 mg/L). The Elovich model explained the kinetics of heterogeneous chemisorption, while PFO and PSO defined adsorption behavior in physisorption and chemisorption, respectively [23]. The Equation of the models is described as follows:

PFO model:
$$\log(q_e - q_t) = log q_e - \frac{k_1}{2.303} t \quad (3)$$

PSO model:
$$\frac{t}{q_t} = \frac{1}{k_2 q_e^2} + \frac{1}{q_e} t \quad (4)$$

Elovich:
$$q_e = \left(\frac{1}{\beta}\right) ln(\alpha\beta) + \left(\frac{1}{\beta}\right) lnt \quad (5)$$

The amount of adsorbed Pb(II) at the time, t, and at equilibrium (mg/g) is described by q_t and q_e, respectively. k_1 and k_2 signify rate constants of the PFO (L/min) and PSO (g/mg·min). While, α represent adsorption rate constant (mg/(g·min)), and β indicates desorption constant (g/mg).

Table 1 lists the linear regression coefficient, R^2, and other calculated parameters. The PSO model was the best model representing the adsorption data owing to its highest R^2 ($\geq$ 0.9943) and closer $q_{e,cal}$ values with $q_{e,exp}$ values. The close match of data with the PSO kinetic model indicates that the reaction is chemisorption, and the reaction rate is proportionate to the number of active sites on the DFSBA-15's surface. Therefore, the fascinating textural properties of DFSBA-15 that consist of fibrous structure could provide better distribution of active sites, thus contributing to the excellent adsorption performance of DFSBA-15. Moreover, the presence of bulk −OH on the DFSBA-15 surface, as evidenced by FTIR analysis (Figure 1(A)), could contribute to the chemisorption adsorption. A comparable finding was also reported by Zhang and a co-worker, where the adsorption of Pb(II) by magnetic polyethyleneimine lignin (M-Lignin-PEI) best fit with the PSO reaction type [24].

Table 1. Isotherm models for Pb(II) adsorption onto DFSBA-15

Models	Parameter	50 mg/L	100 mg/L	200 mg/L	400 mg/L
Experimental	$q_{e,exp}$ (mg/g)	11.14	22.14	43.36	79.65
Pseudo-first-order (PFO)	R^2	0.9662	0.9603	0.9682	0.986
	k_1 (min^{-1})	0.0156	0.0173	0.0152	0.0161
	$q_{e,cal}$ (mg/g)	4.5488	12.712	24.860	61.080
Pseudo-second-order (PSO)	R^2	0.9982	0.9943	0.9944	0.9991
	k_2 (g/mg·min)	9.62E-03	4.24E-03	1.87E-03	6.69E-04
	$q_{e,cal}$ (mg/g)	10.11	20.71	40.75	78.52
Elovich	R^2	0.8669	0.8110	0.8335	0.872
	α (mg/(g.min))	53.397	8.2410	17.244	17.004
	β (g/mg)	0.818	0.2730	0.1427	07017

Isotherm Study

The isotherm models of Freundlich, Temkin, Dubinin-Radushkevich, and Langmuir [25] were applied to analyze the experimental data in this investigation. In a nutshell, Temkin was utilized to explore the impact of adsorbate-adsorbent interactions on the adsorption process [26]. Meanwhile, utilizing the heterogeneous surface theory, the Dubinin-Radushkevich isotherm was ascribed to the adsorption process. In contrast, Langmuir and Freundlich's isotherm explained that monolayer adsorption happens on the homogenous adsorbent's surface and multilayer adsorption over the heterogeneous adsorbent's surface, respectively [27]. These isotherms' linearized forms were stated in Equation (6,7,8,9):

Langmuir:
$$\frac{C_e}{q_e} = \frac{1}{q_m K_L} + \frac{C_e}{q_m} \quad (6)$$

Freundlich:
$$log\ q_e = \log K_F + \frac{1}{n} \log C_e \quad (7)$$

Temkin:
$$q_e = B \ln A + B \ln C \quad (8)$$

Dubinin-Radushkevich:
$$ln\ q_e = ln\ q_m - K_{DR}\,\varepsilon^2 \quad (9)$$

Where adsorption capacity at equilibrium and maximum is described as q_e and q_m (mg/g), respectively. n indicates an empirical constant, and C_e (mg/L) signifies the Pb(II) concentration at equilibrium. In contrast, Langmuir and Freundlich's constants are represented by K_L (L/mg) and K_F ((mg/g)(L/mg)$^{1/n}$), respectively. B signifies Temkin constant, A (L/g) indicates Temkin equilibrium constant, K_{DR} (mol^2/kJ^2) signifies Dubinin-Radushkevich constant, and ε (J/mol) represents Polanyi potential.

Table 2 depicts the calculated regression coefficient, R^2, and kinetic parameters of the studied models. Data analysis revealed that the Langmuir is the close-matched model for this study, represented by the highest R^2 (0.9982). The close match of data with the Langmuir indicates monolayer adsorption on a uniform surface of DFSBA-15. A similar kinetic model was also reported in the literature [28], where the adsorption of Pb(II), Cd(II), and Cu(II) by SiO_2/kaolinite/Fe_2O_3 was best-fitted Langmuir isotherm.

Table 2. Kinetic parameters for removal of Pb(II) by DFSBA-15

Isotherm	Parameters	Value
Langmuir	R^2	0.9982
	q_m (mg/g)	140.85
	K_L (L/mg)	0.0163
	R_L	0.1178
Temkin	R^2	0.9772
	B (J/mol)	25.648
	A (L/g)	0.2397
Freundlich	R^2	0.9579
	n	4.6041
	K_f (mg/g)(L/mg)$^{1/n}$	1.2767
Dubinin Radushkevich	R^2	0.7151
	q_m (mg/g)	38.559
	K_{ad} (10^{-5})	1

CONCLUSION

The DFSBA-15 was successfully prepared using the microwave-assisted microemulsion method. The characterization of DFSBA-15 using FTIR, BET, and FTIR confirmed the formation of fibrous morphology, moderate surface area (156.46 m^2/g), large pore size (7.95 nm), and bulk -OH. Several factors, including time (min), adsorbent dosage (g/L), initial pH, and initial Pb(II) concentration (mg/L), were examined for Pb(II) adsorption, and the best adsorption performance was attained at 180 min, 1 g/L DFSBA-15 dosage, pH 5, and 100 mg/L initial Pb(II) concentration, with 89.88% adsorption of Pb(II). The Langmuir model was a good match for adsorption isotherm, indicating monolayer adsorption on the homogeneous DFSBA-15's surface. The adsorption data closely matched the PSO kinetic model, which revealed that the reaction rate is proportionate to the number of active sites on the DFSBA-15's surface. In short, DFSBA-15 has demonstrated remarkable performance in treating wastewater containing hazardous heavy metals.

ACKNOWLEDGEMENT

The financial support by Universiti Malaysia Pahang through International Publication Grant (RDU203303), Master Research Scheme (MRS), and Postgraduate Research Scheme (PGRS210316) is acknowledged.

REFERENCES

[1] S. Jeevanantham, A. Saravanan, R. V. Hemavathy, P. S. Kumar, P. R. Yaashikaa, and D. Yuvaraj, "Removal of toxic pollutants from water environment by phytoremediation: A survey on application and future prospects," *Environ Technol Innov*, vol. 13, pp. 264–276, 2019, doi: 10.1016/J.ETI.2018.12.007.

[2] J. Łuczyńska, B. Paszczyk, and M. J. Łuczyński, "Fish as a bioindicator of heavy metals pollution in aquatic ecosystem of Pluszne Lake, Poland, and risk assessment for consumer's health," *Ecotoxicol Environ Saf*, vol. 153, pp. 60–67, 2018, doi: 10.1016/J.ECOENV.2018.01.057.

[3] L. P. Lingamdinne, J. R. Koduru, Y. Y. Chang, and R. R. Karri, "Process optimization and adsorption modeling of Pb(II) on nickel ferrite-reduced graphene oxide nano-composite," *J Mol Liq*, vol. 250, pp. 202–211, 2018, doi: 10.1016/J.MOLLIQ.2017.11.174.

[4] C. Q. Teong, H. D. Setiabudi, N. A. S. El-Arish, M. B. Bahari, and L. P. Teh, "Vatica rassak wood waste-derived activated carbon for effective Pb(II) adsorption: Kinetic, isotherm and reusability studies," *Mater Today Proc*, vol. 42, pp. 165–171, 2019, doi: 10.1016/j.matpr.2020.11.270.

[5] V. H. Nguyen, S. M. Smith, K. Wantala, and P. Kajitvichyanukul, "Photocatalytic remediation of persistent organic pollutants (POPs): A review," *Arab J Chem*, vol. 13, no. 11, pp. 8309–8337, 2020, doi: 10.1016/J.ARABJC.2020.04.028.

[6] J. Wu, T. Wang, J. Wang, Y. Zhang, and W. P. Pan, "A novel modified method for the efficient removal of Pb and Cd from wastewater by biochar: Enhanced the ion exchange and precipitation capacity," *Sci Total Environ*, vol. 754, pp. 142150, 2021, doi: 10.1016/J.SCITOTENV.2020.142150.

[7] E. H. Alosaimi, I. Hotan Alsohaimi, H. M. A. Hassan, Q. Chen, S. Melhi, and A. Abdelaziz Younes, "Towards superior permeability and antifouling performance of sulfonated polyethersulfone ultrafiltration membranes modified with sulfopropyl methacrylate functionalized SBA-15," *Chin J Chem Eng*, 2021, doi: 10.1016/J.CJCHE.2021.09.019.

[8] X. Lei, "Enhanced adsorption of perfluorooctanoate (PFOA) onto low oxygen content ordered mesoporous carbon (OMC): Adsorption behaviors and mechanisms," *J Hazard Mater*, vol. 421, pp. 126810, 2022, doi: 10.1016/J.JHAZMAT.2021.126810.

[9] X. Xu, X. K. Ouyang, and L. Y. Yang, "Adsorption of Pb(II) from aqueous solutions using crosslinked carboxylated chitosan/carboxylated nanocellulose hydrogel beads," *J Mol Liq*, vol. 322, pp. 114523, 2021, doi: 10.1016/J.MOLLIQ.2020.114523.

[10] C. C. Chong, S. N. Bukhari, Y. W. Cheng, H. D. Setiabudi, L. P. Teh, and A. A. Jalil, "Facile synthesis of tunable dendritic fibrous SBA-15 (DFSBA-15) with radial wrinkle structure," *Micro Meso Mater*, vol. 294, pp. 109872, 2020, doi: 10.1016/J.MICROMESO.2019.109872.

[11] C. C. Chong, Y. W. Cheng, S. N. Bukhari, H. D. Setiabudi, and A. A. Jalil, "Methane dry reforming over Ni/fibrous SBA-15 catalysts: Effects of support morphology (rod-liked F-SBA-15 and dendritic DFSBA-15)," *Catal Today*, vol. 375, pp. 245–257, 2021, doi: 10.1016/J.CATTOD.2020.06.073.

[12] S. N. Miskan, R. S. M. Zaki, M. B. Bahari, H. D. Setiabudi, and R. Jusoh, "Recent advances in fibrous catalysts for CO_2 conversion: A short review," *Mater Today Proc*, 2021, doi: 10.1016/J.MATPR.2021.08.310.

[13] C. C. Chong, H. D. Setiabudi, and A. A. Jalil, "Dendritic fibrous SBA-15 supported nickel (Ni/DFSBA-15): A sustainable catalyst for hydrogen production," *Int J Hydrog Energy*, vol. 45, no. 36, pp. 18533–18548, 2020, doi: 10.1016/J.IJHYDENE.2019.05.034.

[14] R. Hasan and H. D. Setiabudi, "Removal of Pb(II) from aqueous solution using KCC-1: Optimization by response surface methodology (RSM)," *J King Saud Univ Sci*, vol. 31, no. 4, pp. 1182–1188, 2019, doi: 10.1016/J.JKSUS.2018.10.005.

[15] M. Y. Shahul Hamid, A. Abdul Jalil, A. F. Abdul Rahman, and T. A. Tuan Abdullah, "Enhanced reactive CO_2 species formation via V_2O_5-promoted Ni/KCC-1 for low temperature activation of CO_2 methanation," *React Chem Eng*, vol. 4, no. 6, pp. 1126–1135, 2019, doi: 10.1039/C8RE00312B.

[16] M. Zhang, "Fabrication of the pod-like KCC-1/TiO_2 superhydrophobic surface on AZ31 Mg alloy with stability and photocatalytic property," *Appl Surf Sci*, vol. 499, pp. 143933, 2020, doi: 10.1016/J.APSUSC.2019.143933.

[17] Z. Bai, J. Wang, and Q. Yang, "Iron doped fibrous-structured silica nanospheres as efficient catalyst for catalytic ozonation of sulfamethazine," *Environ Sci Pollut Res*, vol. 25, no. 10, pp. 10090–10101, 2018, doi: 10.1007/S11356-018-1324-8.

[18] N. Bayal, B. Singh, R. Singh, and V. Polshettiwar, "Size and Fiber Density Controlled Synthesis of Fibrous Nanosilica Spheres (KCC-1)," *Sci Reports*, vol. 6, no. 1, pp. 1–11, 2016, doi: 10.1038/srep24888.

[19] J. Bi, "Enhanced removal of Pb(II) and organics by titanate in a designed simultaneous process," *Sep Purif Technol*, vol. 251, pp. 117339, 2020, doi: 10.1016/J.SEPPUR.2020.117339.

[20] Y. Song, L. Y. Yang, Y. G. Wang, D. Yu, J. Shen, and X. K. Ouyang, "Highly efficient adsorption of Pb(II) from aqueous solution using amino-functionalized SBA-15/calcium alginate microspheres as adsorbent," *Int J Biol Macromol*, vol. 125, pp. 808–819, 2019, doi: 10.1016/J.IJBIOMAC.2018.12.112.

[21] K. Kabra, R. Chaudhary, and R. L. Sawhney, "Effect of pH on solar photocatalytic reduction and deposition of Cu(II), Ni(II), Pb(II) and Zn(II): Speciation modeling and reaction kinetics," *J Hazard Mater*, vol. 149, no. 3, pp. 680–685, 2007, doi: 10.1016/J.JHAZMAT.2007.04.028.

[22] F. Zhao, "A straightforward strategy to synthesize supramolecular amorphous zirconium metal-organic gel for efficient Pb(II) removal," *Chem Eng J*, vol. 407, pp. 126744, 2021, doi: 10.1016/J.CEJ.2020.126744.

[23] A. M. Ealias and M. P. Saravanakumar, "Facile synthesis and characterisation of AlNs using Protein Rich Solution extracted from sewage sludge and its application for ultrasonic assisted dye adsorption: Isotherms, kinetics, mechanism and RSM design," *J Environ Manage*, vol. 206, pp. 215–227, 2018, doi: 10.1016/J.JENVMAN.2017.10.032.

[24] X. Zhang, Y. Li, and Y. Hou, "Preparation of magnetic polyethylenimine lignin and its adsorption of Pb(II)," *Int J Biol Macromol*, vol. 141, pp. 1102–1110, 2019, doi: 10.1016/J.IJBIOMAC.2019.09.061.

[25] I. Langmuir, "The adsorption of gases on plane surfaces of glass, mica and platinum," *J Am Chem Soc*, vol. 40, pp. 1361–1403, 1918.

[26] Y. Liu, Y. Xiong, P. Xu, Y. Pang, and C. Du, "Enhancement of Pb (II) adsorption by boron doped ordered mesoporous carbon: Isotherm and kinetics modeling," *Sci. Total Environ*, vol. 708, pp. 134918, 2020, doi: 10.1016/J.SCITOTENV.2019.134918.

[27] S. Benkaddour, "Removal of reactive yellow 145 by adsorption onto treated watermelon seeds: Kinetic and isotherm studies," *Sustain Chem Pharm*, vol. 10, pp. 16–21, 2018, doi: 10.1016/J.SCP.2018.08.003.
[28] S. K. Sharma and D. D. Agarwal, "Adsorption of Pb(II), Cd(II), and Cu(II) ions onto SiO_2/kaolinite/Fe_2O_3 composites: modeling and thermodynamics properties," *Chem. Inter*, pp. 95–100, 2022, doi: 10.5281/zenodo.6877890.